Laser and Particle Beams (2013), *31*, 141–148.

doi:10.1017/S0263034612000869

Marginally igniting direct-drive target designs for the laser megajoule

V. BRANDON,[1] B. CANAUD,[1] M. PRIMOUT,[1] S. LAFFITE,[1] AND M. TEMPORAL[2]
[1]CEA, DAM, DIF, Arpajon, France
[2]ETSIA, Universidad Politecnica de Madrid, Madrid, Spain

(RECEIVED 26 July 2012; ACCEPTED 30 August 2012)

Abstract

Direct-drive target designs below self-ignition threshold are proposed for the laser megajoule in the context of shock-ignition. Two distinct initial aspect ratios are considered and laser pulses are shaped following a classical Kidder's law in order to achieve an implosion velocity of 300 km/s, an in-fight adiabat close to unity and to maximize the peak areal density. The pulse shapes are adjusted to arrange shock timing at the inner side of the DT fuel. The robustness of the laser pulse is addressed by the means of random variations around the initial Kidder's laws. Correlation matrices show no significant correlations between laser parameters. An admissible envelope of laser pulse is given for both designs in order to warrant more than 80% of the best peak areal density. Variations of laser drive power produce variations of implosion velocities in the range 250–370 km/s. Self-ignition threshold is achieved and thermonuclear energy are produced in the range 3 kJ–27 MJ. Finally, the random procedure shows that it is possible to improve the first deterministic optimization and the laser pulses are given.

Keywords: Implosion velocity; In-fight adiabat; Kidder's laws; Shock-ignition

1. INTRODUCTION

Inertial confinement fusion (ICF) achieves high thermonuclear gain by the implosion of a Deuterium Tritium (DT) spherical shell at high velocities (Nuckolls *et al.*, 1972; Lindl,1995; Atzeni *et al.*, 2004; Lindl *et al.*, 2004). The implosion is driven by X-ray in a conventional indirect-drive approach (Lindl *et al.*, 2004; Giorla *et al.*, 2006; Laffite *et al.*, 2010; Lan *et al.*, 2012) or by direct laser beams (Nuckolls *et al.*, 1972; Bodner *et al.*, 2002; Canaud *et al.*, 2004*a*). The usual pellet contains solid DT layer that requires cryogenic system (Perin, 2010). The implosion stands in three distinct steps named the acceleration, the deceleration, and the stagnation. The deceleration begins when the implosion velocity of the shell reaches a maximum whereas the stagnation occurs when the implosion velocity vanishes. During this stage, the shell is highly compressed up to 4000 times its initial solid density while the central part is strongly pressured and heated and becomes the hot spot. When the hydrodynamics conditions are achieved, a thermonuclear burn wave takes place in the central part and propagates toward the dense cold fuel. The thermonuclear energy delivered in this stage becomes much more greater than the driver energy employed to compressed the target. The thermodynamics conditions required to generate and sustain such burn waves are strongly connected to the maximum kinetic energy of the pellet achieved during implosion, just after the end of the laser pulse. When this kinetic energy is above a particular value, named kinetic or self-ignition threshold, thermodynamics conditions allow thermonuclear ignition and burn. At the opposite, the shell decelerates and rebounds while, in the central part, thermonuclear fusion reactions take place without delivering a big amount of energy. This case corresponds to marginally igniting targets and could be ignited by shock ignition (Betti *et al.*, 2007; Ribeyre *et al.*, 2009; Canaud *et al.*, 2010; 2011; 2012; Eliezer *et al.*, 2011), impact ignition (Murakami, 2006; Azechi, 2009), or fast-ignition (Basov *et al.*, 1992; Tabak *et al.*, 1994; Tabak *et al.*, 2005; Atzeni *et al.*, 2007; Willi *et al.*, 2000; Deutsch *et al.*, 2011). Implosion dynamics of capsule and thermonuclear gain are directly related to the twin set of target and laser pulse. Kidder-like laser pulse shape (Kidder,1976) is traditionally used to directly drive the implosion of the target. Unfortunately, direct-drive does not allow shockless implosion and the isentropic compression is done while few

Address correspondence and reprint requests to: B. Canaud, CEA, DAM, DIF, F-91297 Arpajon, France. E-mail: benoit.canaud@cea.fr

shock propagate in the shell. Thus, each point of laser pulse shape is chosen to optimize shock timing at the interface of DT cryogenic and DT gas in order to keep the shell adiabat as constant as possible. This means that one target is designed by a twin set of size and laser pulse for an implosion velocity and an in-flight adiabat coefficient (defined as the ratio of shell pressure over fermi pressure). Usually, in order to change implosion velocity, the drive is modified.

However, the optimization of the laser pulse, usually done by adjusting shock timing, has to be correlated to final implosion stage and its observables such as the peak shell areal density or the thermonuclear energy. A fussy optimization of these lasts should lead to a modified pulse shape.

Another question concerns the influence of the laser ramp shape on the compression (areal density, thermonuclear yield...) of the target when the laser pulse departs from the Kidder-like law. Indeed, even if, Kidder's law allows to adjust the shock timing, the knowledge of the influence of temporal laser profile depends on the design defined. Indeed, the sensitivity of the design to small variations due to laser errors such as power imbalance or pointing errors is currently addressed in a multidimensional approach (Murakami *et al.*, 1993; Canaud *et al.*, 2002; Temporal *et al.*, 2009; 2010*a*; 2010*b*; Canaud *et al.*, 2012). One-dimensional effect can also be considered by summing errors over the whole solid angle. The resulting laser power should depart perturbatively from the perfect laser pulse shape especially during the ramp. A modification of shock timing induced by these perturbations can, in a certain manner, be deleterious for the achievement of the thermonuclear gain and fusion requirements.

Analysis of the design response to small perturbations of the laser pulse shape should give an estimate of the robustness of the design. Our laser pulse ramp is usually defined with seven different points (twin set of power and time) and a systematic variation of points (in a 14 dimension space) in an interval centered on the nominal values should lead to more than few millions of hydrodynamics calculations. Such an approach should be tedious and time consuming. An alternative way (Primout, 2004) consists in randomly exploring the vicinity of Kidder's law and in establishing cross-correlation of laser parameters. This should reduce the total number of calculations to few thousands.

In addition, this should improve the laser pulse shape in comparison to the Kidder's law and, in the same time, the drive power variation would lead to explore a wide interval of implosion velocity.

Our work is done in the context of the laser megajoule (LMJ) (Lion, 2010) and the National Ignition Facility (NIF) completion and the quest for high gain inertial fusion (Moses, 2012). This paper addresses the response of a baseline direct-drive design to random variations of its Kidder's like laser pulse ramp. Our approach concerns new designs to whom implosion velocities (in the range 250–370 km/s) are lower than the ones currently encountered in conventional direct drive (Canaud *et al.*, 2007; McKenty *et al.*, 2004) or indirect drive fusion (Lindl *et al.*, 2004; Giorla *et al.*, 2006; Laffite *et al.*, 2010). These new designs could be used for shock ignition or fast-ignition.

The paper is organized as follow. The first section introduces baseline designs. A random walk optimization method is presented in the next section. It is based on one-dimensional numerical calculation of target implosion. Input and output parameters are given for two distinct targets defined by an initial aspect ratio of 3 and 5. Then, the third section is devoted to the analysis of the numerical results while the last section focuses on the consequences of random realization of target designs.

2. DIRECT-DRIVE DESIGNS

We consider spherical cryogenic DT layer at density of 250 kg/m^3 surrounding a central DT gas (with a density $\rho = 0.3\ kg/m^3$) with a thick CH overcoat ($\rho = 1070\ kg/m^3$) in order to improve the laser absorption (Canaud *et al.*, 2004*b*) in comparison to the All-DT material (McKenty *et al.*, 2004; Atzeni *et al.*, 2007). DT fuel mass (roughly 300 μg) is similar to payload fuel masses currently encountered in ICF (Laffite *et al.*, 2010; Atzeni *et al.*, 2007). The CH thickness is chosen large enough to keep small dense layer at the end of the laser pulse. The target dimensions explore two distinct initial aspect ratios A (defined as the DT-ice inner radius over the DT-ice thickness) A = 3 and A = 5 (Fig. 1). In comparison, HiPER target (Atzeni *et al.*, 2007) have an initial aspect ratio of ~7 in considering only payload fuel for fast ignition. Direct drive target for laser megajoule (Canaud *et al.*, 2004*b*) is defined with an initial aspect ratio of ~7.7. Recent studies (Schmitt *et al.*, 2009; Bates *et al.*, 2010) propose target with an initial aspect ratio of ~2.1 for shock ignition.

For a given laser energy, a lower initial aspect ratio leads to a lower implosion velocity and combined with a larger thickness this should lead to a better hydrodynamic stability. Assuming a best burn fraction of 30%, 300 μg mass should deliver a thermonuclear energy around 25 MJ.

Kidder-like laser pulses (cf Fig. 2) present three distinct parts: the foot, the ramp, and the drive. The foot, at a low laser power level, creates a first shock in the capsule which places the fuel on the right in-flight adiabat $\alpha_{if} = P[MPa]/2.17\rho^{5/3}[kg/m^3] \sim 1.2$. Here, we consider an ablation pressure (P_a) during foot of 300 GPa produced by a foot laser power lower than 1 TW. The second part of laser pulse is the ramp-up. Its goal is to increase the external imploding pressure without increasing the internal energy of the DT shell while successive shocks are sent through out the spherical pellet. They emerge to the inner target side at successive times and the ramp is built to adjust time delay at roughly 0.3 ns. This particularly ramp produces a quasi-isentropic compression, and α_{if} stays close to 1 during the acceleration phase. The drive part of the laser pulse is the maximum laser power plateau which gives the desired implosion velocity of the shell. The laser pulses

https://doi.org/10.1017/S0263034612000869 Published online by Cambridge University Press

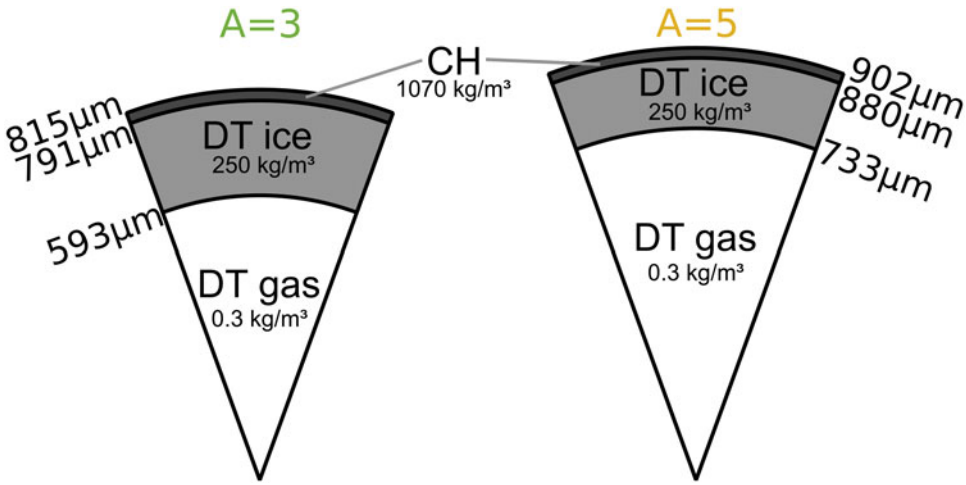

Fig. 1. Target design : A = 3 (left) and A = 5 (right).

shown on Figure 2 produce a peak implosion velocity close to 300 km/s and reach peak areal densities of 18 kg/m^2 and 13 kg/m^2 for A = 3 and A = 5, respectively. Peak areal density ρR is defined as the maximum of areal density reached during the implosion and especially during the deceleration phase. Designs do not ignite.

These laser pulses are the starting point of our study presented here. Criteria used to quantify properly the laser pulse modifications are the peak areal density under the self-ignition threshold and the maximum thermonuclear energy above it using minimum incident energy.

Calculations are performed using the one-dimensional (1D) Lagrangian radiation-hydrodynamics code: FCI 1D (Buresi *et al.*, 1986). It includes tabulated equations of state (e.g., SESAME), flux-limited Spitzer heat transport (here the flux limiter is set at 6%), multi-group radiative transfer, 1D normal-incidence ray-tracing with refraction, multi-group alpha-particle transport, and neutron transport.

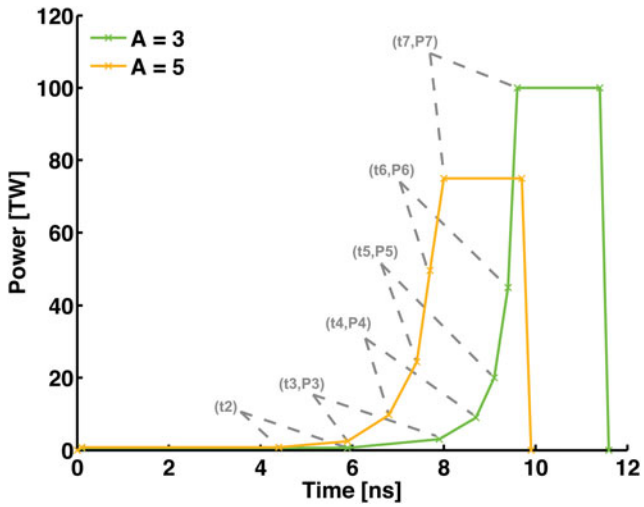

Fig. 2. Kidder-like laser pulses associated to both targets defined in Fig. 1.

Degeneracy of the fuel during the deceleration is taken into account in the thermal conductivity using a harmonic average between Spitzer and the Hubbard (1966) model that is validated by quantum molecular dynamics calculations (Recoules *et al.*, 2009).

3. RANDOM PROCEDURE

The method is based on a random Monte Carlo procedure. Each point of the laser pulse ramp defined in Figure 2 is chosen randomly in order to generate new laser pulse shapes. Previous studies have shown that it is very efficient in many different problems of optimization (Primout, 2004; Canaud *et al.*, 2004*b*; 2004*a*) in large-dimension space of parameters. All points are perturbed randomly around their initial positions in a defined intervals to shape a new laser pulse. Nevertheless, the drive duration is kept constant at 1.8 ns.

Because the foot power and the drive duration are given, there are six random times and five random laser powers. Time intervals can not overlap and laser power of first points is limited to low level. We have also relaxed the drive power and thus implosion velocity should change. About 3000 computations have been realized for each target in a first run with large intervals to cover large implosion velocities. Then, we employed a refinement method to explore specific or underpopulated areas. Successive refinements are realized by adjusting intervals boundaries of parameters. This is done by following the evolution of each time and power points in function of results. By doing this, we notice that the previous results obtained by using a Kidder's law can be improved and an ideal value of each input parameter can be obtained. The parametric space of results is meshed with a regular grid and we estimate an average value in each cell. We follow for each input parameters (time and power) its trend in function of implosion velocity, thermonuclear energy, areal density, and incident energy.

https://doi.org/10.1017/S0263034612000869 Published online by Cambridge University Press

This method requires enough points on boundaries of output data space to be efficient. For instance, Figure 3 represents the trend of the time t_4 as a function of the thermonuclear energy and the implosion velocity space.

Results of these successive random realizations are the clouds shown in Figure 4. These figures present the thermonuclear energy and the peak areal density in function of implosion velocity, and the absorbed energy in function of areal density for both initial aspect ratios. More than 5000 hydrodynamic calculations have been realized. Each point is the result of a computation for a new laser pulse shape. Implosion velocities cover a range from 250 km/s to 370 km/s. The peak areal density spreads from 1 to 19 kg/m^2 while the absorbed energy from 150 to 300 kJ. We also observe that the thermonuclear energy covers a wide range between 1 kJ and 30 MJ. It can be seen also, in the last case, a transition between marginally and self-igniting target designs which deliver high thermonuclear energy.

Bounds of intervals have to be chosen correctly in order to not truncate the space of result. Criteria used are the peak areal density under the self-ignition threshold and the thermonuclear energy above. A threshold value at 90% of $(\rho R)_{max}$ is fixed for all computation results. First, we checked that computations cover the most uniformly all parameter intervals and, then, the refinement method changed the interval boundaries. Thus, extreme parts of interval are under populated. The histogram of all computations for all superposed intervals (full and refined ones) shows that interval boundaries are under populated. However, it is not a crucial problem as far as the maximum number of computations satisfying the areal density criteria is not close to boundaries of the interval. Such measurement represents a kind of distribution function of parameters satisfying the optimization criteria and this distribution function must have a peak centered on the center of the parameter range in order to cover all optima possibilities.

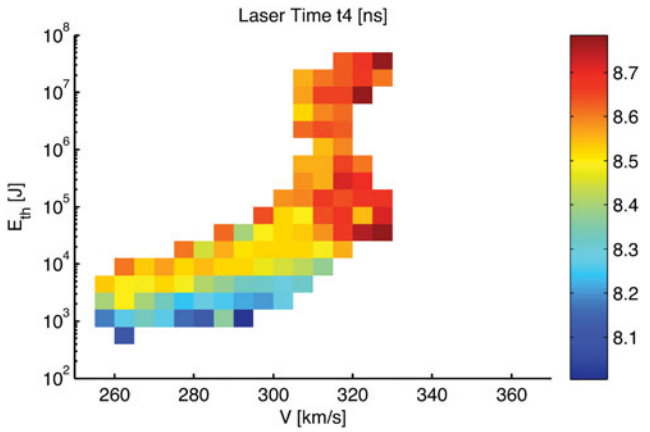

Fig. 3. Example of the refinement method used : trend of an input parameter (time t4 in ns on this figure) for A = 3 target as a function of implosion velocity (V) and thermonuclear energy (E_{Th}). If time t4 increase in interval represented, implosion velocity and thermonuclear energy increase. If we want to explore specific area, it needs to select values refered by this method. This analysis is realized on each random time and power, and allows to define efficient refinements in function of areas to explore.

As an example, we represent in Figure 5 the distribution function for all random realizations of parameter t_4 [ns] as well as for the selected realizations that satisfy the criteria of 90% of $(\rho R)_{max}$. The full-realization distribution function has a maximum due to the successive refinements done during the optimization process. The selected distribution function, for parameters satisfying the criteria $\rho R \geq 90\%$ $(\rho R)_{max}$, is also represented (in orange). It can be seen also that the peak of the selected distribution is roughly centered on the parameter interval of realization. We checked this for all parameters.

4. ANALYSIS OF THE RANDOM REALIZATIONS

The Monte-Carlo procedure has produced a wide variety of target designs covering implosion velocities from 260 to 370 km/s. The interest of such approach is that the results consist in a data base of imploding targets with different implosion specificities. A comparison between two different class of targets, referenced by their initial aspect ratio is now available. In a first step, we focus on the correlations between input and output data by the mean of a correlation matrix

4.1. Correlation matrix

A first matrix B of $N \times 17$ parameters is built, N being the number of random realizations. For each aspect ratio, the input and output data are summarized as following: six times (t_2 to t_7), five powers (P_3 to P_7) , peak density (ρ), peak areal density (ρR), peak ionic temperature (T_i), peak implosion velocity (V), absorbed energy (E_A), and thermonuclear energy (E_{th}):

$$B = \begin{pmatrix} t_2 & \cdots & P_7 & \rho & \rho R & T & V & E_a & E_{Th} \\ b_{1,1} & \cdots & b_{1,11} & b_{1,12} & b_{1,13} & b_{1,14} & b_{1,15} & b_{1,16} & b_{1,17} \\ b_{2,1} & \cdots & b_{2,11} & b_{2,12} & b_{2,13} & b_{2,14} & b_{2,15} & b_{2,16} & b_{2,17} \\ \vdots & \ddots & \vdots & \vdots & \vdots & \vdots & \vdots & \vdots & \vdots \\ b_{N,1} & \cdots & b_{N,11} & b_{N,12} & b_{N,13} & b_{N,14} & b_{N,15} & b_{N,16} & b_{N,17} \end{pmatrix} \quad (1)$$

We then build the square correlation matrix C:

$$C = \begin{pmatrix} t_2 & \cdots & P_7 & \rho & \rho R & T & V & E_a & E_{Th} \\ 1 & \cdots & c_{1,11} & c_{1,12} & c_{1,13} & c_{1,14} & c_{1,15} & c_{1,16} & c_{1,17} \\ c_{2,1} & \cdots & c_{2,11} & c_{2,12} & c_{2,13} & c_{2,14} & c_{2,15} & c_{2,16} & c_{2,17} \\ \vdots & \ddots & \vdots & \vdots & \vdots & \vdots & \vdots & \vdots & \vdots \\ c_{17,1} & \cdots & c_{17,11} & c_{17,12} & c_{17,13} & c_{17,14} & c_{17,15} & c_{17,16} & 1 \end{pmatrix}, \quad (2)$$

with $c_{i,j} = c_{j,i}$ for $i \neq j$, $c_{i,i} = 1$, and $c_{i,j} = \frac{\sigma^2_{i,j}}{\sqrt{\sigma^2_{i,i}\sigma^2_{j,j}}}$. $\sigma^2_{i,j}$ are the covariance elements:

https://doi.org/10.1017/S0263034612000869 Published online by Cambridge University Press

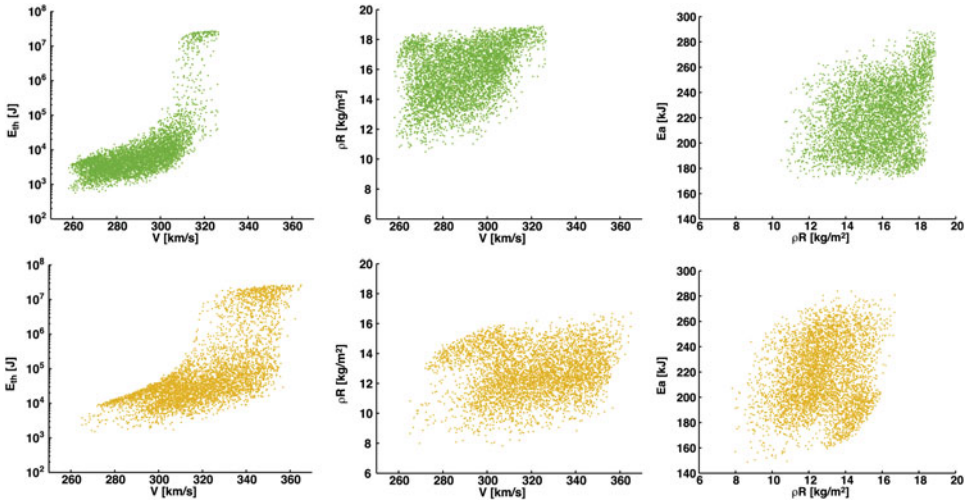

Fig. 4. Results of successive refinement for A = 3 (top) and A = 5 (bottom): thermonuclear energy (left) and areal density vs implosion velocity (center), and absorbed energy as a function of areal density (right).

$$\sigma^2_{i,j} = \frac{1}{N-1}\sum_{n=1}^{N}(b_{n,i} - \bar{b}_i)(b_{n,j} - \bar{b}_j). \quad (3)$$

where $\bar{b}_i = \sum_{j=1}^{N} b_{j,i}/N$ is the average of $b_{j,i}$ over the random realizations.

We used the same criteria than previously on the peak areal density to compute correlation coefficients. Laser pulse shapes that give more than 90% of the maximum peak areal density are selected. For A = 3, computations give more than 2000 samples that reach a peak areal density greater than 16 kg/m^2 while for A = 5, only 1000 random realizations produce a peak areal density greater than 14 kg/m^2 and are used to compute correlation matrix .

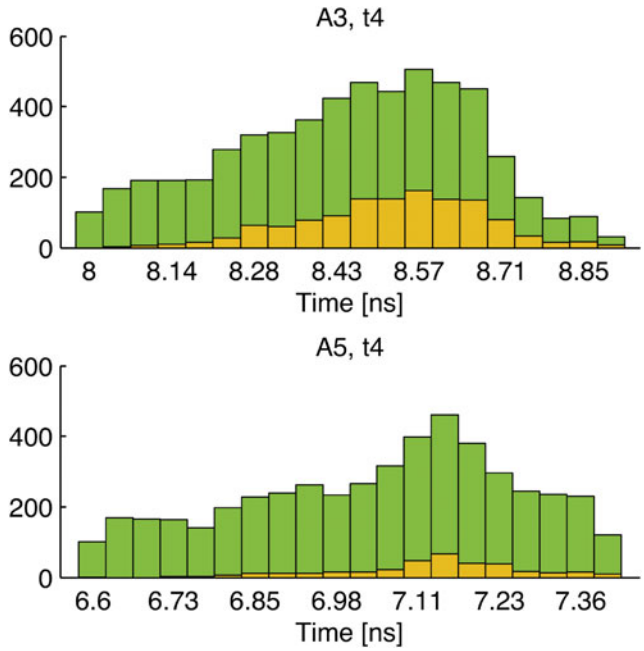

Fig. 5. Example of histograms traced to verify the validity of intervals refinements for the fourth time t_4 [ns] (top: A = 3, bottom: A = 5). Green part represents all random realizations while orange one represents the part of results that have areal density greater than 90% of maximum areal density.

Correlation matrices are shown in Figure 6 for both initial aspect ratio. Coefficients are normalized to unity and higher the matrix coefficient, stronger the correlation is. For both initial aspect ratio, there are no specific correlations in the input parameter space (times and laser powers). However, if we look at the areal density, there is a slight correlation with P6, t7, and anti-correlation with t6, in other word, there is a correlation of areal density with higher energy before drive. A correlation between drive power (P7) and implosion velocity, and with the absorbed energy is confirmed, as it could be predicted. Similarly to the correlation between thermonuclear energy and temperature, densities and areal densities are, also, strongly correlated.

However, correlations are different between A = 3 and A = 5. For A = 3, density is mainly linked to areal density and slightly to the temperature and thermonuclear energy. For A = 5, density is first linked to the thermonuclear energy, and after to the temperature, and the areal density. Finally, thermonuclear energy appears to be more sensitive to others output data for A = 5 than for A = 3. This sensitivity is not well understood and calculations should have to be performed to have a clearest explanation. However, one possible explanation comes from the relative number of high gain realizations. In the case A = 5, there are more realizations above the ignition threshold than in the case A = 3. As the target ignites, all the hydrodynamics data (temperatures, peak densities and peak areal densities) are affected by the thermonuclear reactions which alter the deceleration and stagnation stages. Thus, correlations between all these hydrodynamic data are amplified. This could be the

https://doi.org/10.1017/S0263034612000869 Published online by Cambridge University Press

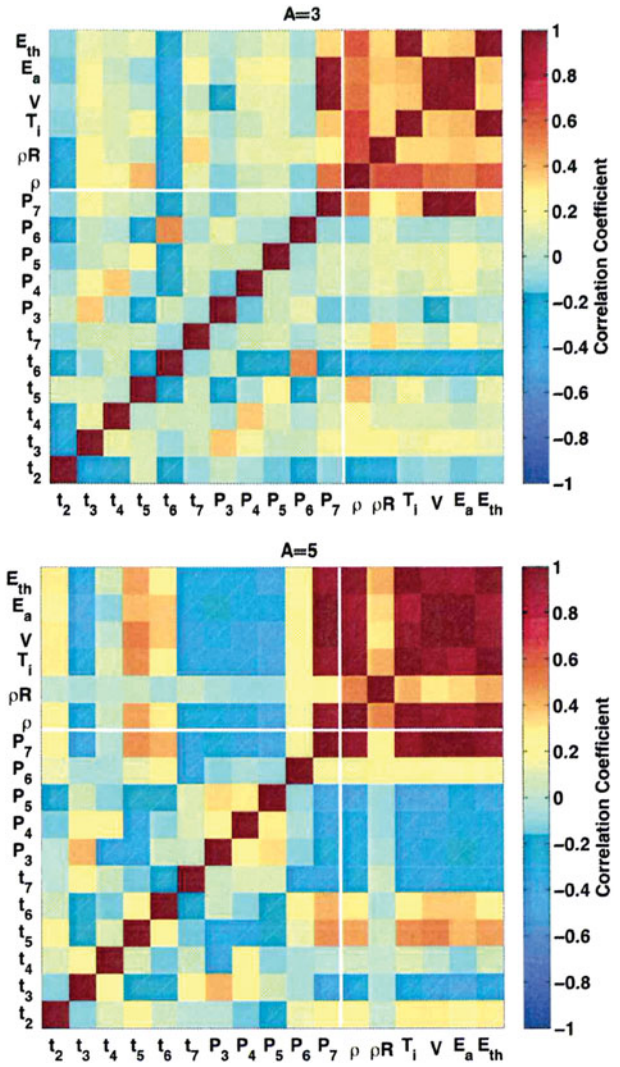

Fig. 6. Correlation matrix (C) computed for results areal density upper than 90% of $(\rho R)_{max}$ for each aspect ratio (top: A = 3, bottom: A = 5), as a function of the input (t_i, P_i) and output (ρ, ρR, T, V, E_a, E_{Th}) parameters.

reason why the sensitivity of the case A = 5 is higher than for A = 3.

4.2. Effects on target designs

We now address the results from the target design point of view. The first consequence that we observe is that the maximum areal density can still be improved in comparison to the first optimization done for the A = 5-design while for A = 3, the optimum seems reached. Finally, results are still Kidder-like laser laws but the shock timing could be different.

The case A = 5 is rather different than A = 3. We can remark that optimized A = 5 laser pulse shape obtained from the random method are similar to Kidder's law but with longer and less powered laser pulses as seen in Figure 7. The areal density evolves from 13 kg/m^2 to 16 kg/m^2 for the first Kidder's law and the randomized Kidder's law optimizations respectively. These results seem to indicate that Kidder's like law has to be modified and adjusted in oder to obtain highest areal densities while keping the same in-flight adiabat and implosion velocity. On another hand, for A = 3, we did not observe such kind of behavior. Indeed, the random calculations show an optimal drive duration of the same order than the initial optimization done by shock timing. We have not developed further this aspect because it is out of the scope of the paper but this axis of investigation is interesting because it implies that the optimal drive duration could be dependent on the initial aspect ratio.

From the correlation matrices, it can be also concluded that when laser ramps vary randomly inside an area defined by the criteria $\rho R \geq 0.9\rho R_{max}$, there are no specific correlations between the points in the ramp and with the implosion characteristics (for a given implosion velocity). This gives the tolerance of the target design to random fluctuation of the laser facility. The criteria $\rho R \geq 0.9\rho R_{max}$, for a given implosion velocity, leads to tolerances on each point of laser ramp (cf Fig. 7). It is almost the same for different implosion velocities but rather different between A = 3 and A = 5.

These tolerances are summarized in Table 1 which gives the twin set of laser pulse points for the optimization and both envelopes, defining the upper and the lower limits of the requirement $\rho R \geq 0.9\rho R_{max}$.

That means that every laser pulse exploring the grey part of Figure 7 should drive an implosion at a peak velocity of 300 ± 3 km/s and a peak areal density of 18 ± 1 kg/m^2 and 15 ± 1 kg/m^2 for A = 3 and A = 5, respectively.

A last aspect concerns the variation of the implosion velocity with the drive power. When this last varies while the ramp stands in its optimized area, the total ablated mass and the total payload mass are not constants and consequently the peak implosion velocity varies. In all previous calculations, we warrant that the fuel mass is not impacted by laser energy. At the end of the laser pulse, it is possible that residual mass of CH is still present. The maximum peak areal densities stay close to 19 kg/m^2 and 16 kg/m^2 for A = 3 and A = 5, respectively, when the implosion velocity varies. Thicker the target, higher the peak areal density is, for fixed implosion velocity. Self-ignition threshold is easily seen for both targets on left frames. For A = 3, self-ignition threshold is around 305 km/s and 320 km/s for A = 5. As fuel mass is constant, variation of implosion velocity is equivalent to a kinetic energy variation. The kinetic energy threshold of self-ignition is lower for A = 3 than A = 5.

5. CONCLUSION

Two different target designs are presented here with initial aspect ratios of A = 3 and A = 5 with a payload DT mass of 300 μg. A first optimization of a Kidder-like law for the laser pulse is done by adjusting shock timing at the inner side of the DT ice layer. A random variation of the pulse ramp is done in order to check the sensitivity of designs to their laser shape. This random walk method is addressed by

https://doi.org/10.1017/S0263034612000869 Published online by Cambridge University Press

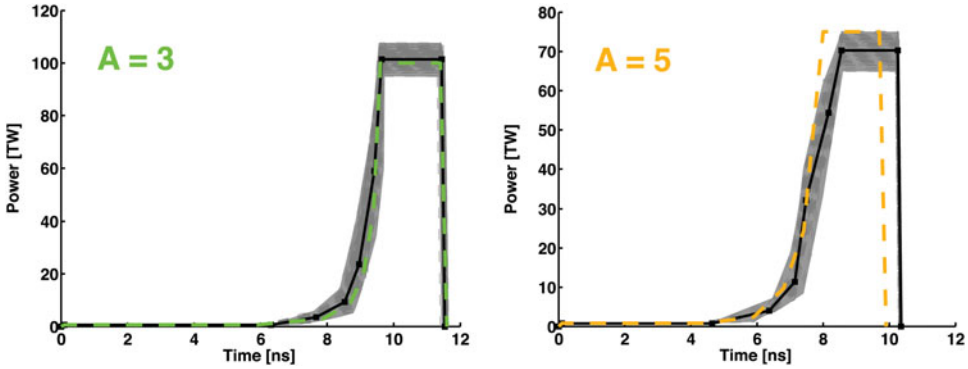

Fig. 7. Initial (dashed lines), optimized (dark square) laser pulses and optimization area (in grey) generated by random realizations.

Table 1. *List of twin set of times (in ns) and powers (in TW) for optimized (opt.) and envelope (min and max) laser pulses for an implosion velocity of 300 km/s*

A = 3						A = 5					
opt.		max		min		opt.		max		min	
t	P	t	P	t	P	t	P	t	P	t	P
0	0	0	0	0	0	0	0	0	0	0	0
0.1	0.6	0.1	0.6	0.1	0.6	0.1	0.74	0.1	0.74	0.1	0.74
6.4	0.6	6.1	0.6	6.7	0.6	4.6	0.74	4.5	0.74	4.8	0.74
7.7	3.5	7.4	4.7	7.9	2.4	6.4	4	6.1	4.9	6.5	2.6
8.53	9.31	8.3	13	8.7	7.2	7.1	11	7	13	7.3	9
9	24	8.8	28	9.1	19	7.5	32	7.4	36	7.6	25
9.4	59	9.3	72	9.6	46	8.2	54	8.1	60	8.3	50
9.64	101	9.6	105	9.7	98	8.6	70	8.5	73	8.6	68
11.4	101	11.4	105	11.5	98	10.3	70	10.2	73	10.3	68
11.5	0	11.5	0	11.6	0	10.4	0	10.3	0	10.4	0

the way of many thousand calculations. It is shown that this method leads to a better laser pulse shape to reach the maximum of the peak areal density for a given implosion velocity. This optimized laser pulse shape is very close to the previous one for A = 3 while its drive part is significantly time enlarged and power lowered for the target A = 5. A random variation of the peak power of the laser pulse leads to cover a wide range of implosion velocities (between 250 and 370 km/s), absorbed laser energies (160–300 kJ) and thermonuclear energies (3 kJ–27 MJ). Self-ignition threshold is explored for both initial aspect ratios, and we show that this threshold is achieved with lower implosion velocity for smaller initial aspect ratio. Finally, an optimized laser pulse shape is proposed for both initial aspect ratio with upper and lower bounds. In the future, for each initial aspect ratio, we plane to use these baseline designs to perform shock ignition in the context of the French Laser MegaJoule facility (Canaud *et al.*, 2010).

REFERENCES

Atzeni, S. & Meyer-Ter-Vehn, J. (2004). *Inertial Fusion: Beam Plasma Interaction, Hydrodynamics, Dense Plasma Physics*. Oxford: Oxford Science Publications.

Atzeni, S., Schiavi, A. & Bellei, C. (2007). Targets for direct-drive fast ignition at total laser energy of 200–400 kJ. *Phys. Plasmas* **14**, 2702.

Azechi, H., Sakaiya, T., Watari, T., Karasik, M., Saito, H., Ohtani, K., Takeda, K., Hosoda, H., Shiraga, H., Nakai, M., Shigemori, K., Fujioka, S., Murakami, M., Na-gatomo, H., Johzaki, T., Gardner, J., Colombant, D.G., Bates, J.W., Velikovich, A.L., Aglitskiy, Y., Weaver, J., Obenschain, S., Eliezer, S., Kodama, R., Norimatsu, T., Fujita, H., Mima, K. & Kan, H. (2009). Experimental evidence of impact ignition: 100-fold increase of neutron yield by impactor collision. *Phys. Rev. Lett.* **23**, 235002–235006.

Basov, N., et al. (1992). *Soviet Laser Res.* **13**, 396.

Bates, J.W., Schmitt, A.J., Fyfe, D.E., Obenschain, S.P. & Zalesak, S.T. (2010). Simulations of high-gain shock-ignited inertial-confinement-fusion implosions using less than 1 MJ of direct KrF-laser energy. *Hi. Ener. Density Phys.* **6**, 128–134.

Betti, R., Zhou, C.D., Anderson, K.S., Perkins, L.J., Theobald, W. & Solodov, A.A. (2007). Shock ignition of thermonuclear fuel with high areal density. *Phys. Rev. Lett.* **98**, 155001.

Bodner, S.E., Colombant, D.G., Schmitt, A.J., Gardner, J.H., Lehmberg, R.H. & Obenschain, S.P. (2002). Overview of new high gain target design for a laser fusion power plant. *Fusion Engin. Design* **60**, 93–98.

https://doi.org/10.1017/S0263034612000869 Published online by Cambridge University Press

Buresi, E., Coutant, J., Dautray, R., Decroisette, M., Duborgel, B., Guillaneux, P., Launspach, J., Nelson, P., Patou, C., Reisse, J.M. & Watteau, J.P. (1986). Laser program development at CEL-V: Overview of recent experimental results. *Laser Part. Beams* **4**, 531.

Canaud, B. & Temporal, M. (2010). High-gain shock ignition of direct-drive ICF targets for the laser megajoule. *New J. Phys.* **12**, 3037, 2010.

Canaud, B., Brandon, V., Laffite, S. & Temporal, M. (2012). 2D analysis of direct-drive shock-ignited HiPER-like target implosions with the full laser megajoule. *Laser Part. Beams* **30**, 183–189.

Canaud, B., Fortin, X., Dague, N. & Bocher, J.L. (2002). Laser megajoule irradiation uniformity for direct drive. *Phys. Plasmas* **9**, 4252–4260.

Canaud, B., Fortin, X., Garaude, F., Meyer, C. & Philippe, F. (2004*a*). Progress in direct-drive fusion studies for the laser megajoule. *Laser Part. Beams* **22**, 109–114.

Canaud, B., Fortin, X., Garaude, F., Meyer, C., Philippe, F., Temporal, M., Atzeni, S. & Schiavi, A. (2004*b*). High-gain direct-drive target design for the laser megajoule. *Nucl. Fusion* **44**, 1118–1129.

Canaud, B., Garaude, F., Clique, C., Lecler, N., Masson, A., Quach, R. & Van der Vliet, J. (2007). High-gain direct-drive laser fusion with indirect drive beam layout of laser megajoule. *Nuclear Fusion* **47**, 1652–1655.

Canaud, B., Laffite, S. & Temporal, M. (2001). Shock ignition of direct-drive double-shell targets. *Nucl. Fusion* **51**.

Deutsch, C. & Didelez, J.P. (2011). Inertial confinement fusion fast ignition with ultra-relativistic electron beams. *Laser Part. Beams* **29**, 39–44.

Eliezer, S. & Martinez Val, J.M. (2011). The comeback of shock waves in inertial fusion energy. *Laser Part. Beams* **29**, 175, 2011.

Giorla, J., Bastian, J., Bayer, C., Canaud, B., Casanova, M., Chaland, F., Cherfils, C., Clique, C., Dattolo, E., Fremerye, P., Galmiche, D., Garaude, F., Gauthier, P., Laffite, S., Lecler, N., Liberatore, S., Loiseau, P., Malinie, G., Masse, L., Masson, A., Monteil, M.C., Poggi, F., Quach, R., Renaud, F., Saillard, Y., Seytor, P., Vandenboomgaerde, M., Van der Vliet, J. & Wagon, F. (2006). Target design for ignition experiments on the laser megajoule facility. Plasma physics and controlled marginally igniting direct-drive target designs for the laser megajoule. *Fusion* **48**, B75–B82.

Hubbard, W.B. (1966). Studies in stellar evolution. v. transport coefficients of degenerate stellar matter. *Astrophys. J.* **146**, 858.

Kidder, R.E. (1976). Energy gain of laser-compressed pellets — A simple model calculation. *Nucl. Fusion* **16**, 405–408.

Laffite, S. & Loiseau, P. (2010). Design of an ignition target for the laser megajoule, mitigating parametric instabilities. *Phys. Plasmas* **17**, 102704.

Lan, K., Lai, D., Zhao, Y. & Li, X. (2012). Initial study and design on ignition ellipraum. *Laser Part. Beams* **30**, 175–182.

Lindl, J. (1995). Development of the indirect-drive approach to inertial confinement fusion and the target physics basis for ignition and gain. *Phys. Plasmas* **2**, 3933–4024.

Lindl, J.D., Amendt, P., Berger, R.L., Glendinning, S.G., Glenzer, S.H., Haan, S.W., Kauffman, R.L., Landen, O.L. & Suter, J. (2004). The physics basis for ignition using indirect-drive targets on the national ignition facility. *Phys. Plasmas* **11**, 339–491.

Lion, C. (2010). The LMJ program: An overview. *J. Phys.* **244**, 012003–012010.

McKenty, P.W., Sangster, T.C., Alexander, M., Betti, R., Craxton, R.S., Delettrez, J.A., Elasky, L., Epstein, R., Frank, A., Glebov, V.Yu., Goncharov, V.N., Harding, D.R., Jin, S., Knauer, J.P., Keck, R.L., Loucks, S.J., Lund, L.D., McCrory, R.L., Marshall, F.J., Meyerhofer, D.D., Regan, S.P., Radha, P.B., Seka, W., Skupsky, S., Smalyuk, V.A., Soures, J.M., Thorp, K.A., Wozniak, M., Frenje, J.A., Li, C.K., Petrasso, R.D., Seguin, F.H., Fletcher, K.A., Padalino, S., Freeman, C., Izumi, N., Koch, J.A., Lerche, R.A., Moran, M.J., Phillips, T.W., Schmid, G.J. & Sorce, C. (2004). Direct-drive cryogenic target implosion performance on OMEGA. *Phys. Plasmas* **11**, 2790–2797.

Moses, E. (2012). The National Ignition Facility: status and progress towards fusion ignition. *Fusion Sci. Techn.* **61**, 3–8.

Murakami, M., Nagatomo, H., Azechi, H., Ogando, F., Perlado, M. & Eliezer, S. (2006). Innovative ignition scheme for ICF-impact fast ignition. *Nucl. Fusion* **46**, 99–103.

Murakami, M., Nishihara, K. & Azechi, H. (1993). Irradiation nonuniformity due to imperfections of laser beams. *J. Appl.Phys.***74**, 802–808.

Nuckolls, J., Wood, L., Thiessen, A. & Zimmerman, G. (1972). Laser compression of matter to super-high densities: Thermonuclear (CTR) applications. *Nat.* **239**, 139–142.

Perin, J.P. (2010). Cryogenic systems for LMJ cryotarget and HiPER application. *Laser Part. Beam* **28**, 203.

Primout, M. (2004). Optimization of X-ray conversion efficiency of laser-preformed metallic plasma. *J. X-ray Sci. Techn.* **13**, 23–36.

Recoules, V., Lambert, F., Decoster, A., Canaud, B. & Clerouin, J. (2009). AbInitio determination of thermal conductivity of dense hydrogen plasmas. *Phys. Rev. Lett.* **102**, 75002.

Ribeyre, X., Schurtz, G., Lafon, M., Galera, S. & Weber, S. (2009). Shock ignition: An alternative scheme for HiPER. *Plasma Phys. Contr. Fusion* **51**, 5013.

Schmitt, A.J., Bates, J.W., Obenschain, S.P., Zalesak, S.T., Fyfe, D.E. & Betti, R. (2009). Direct drive fusion energy shock ignition designs for Sub-MJ lasers. *Fusion Sci. Techn.* **56**, 377–383.

Tabak, M. & Callahan, D. (2005). Models of gain curves for fast ignition. *Nucl. Instr. Meth. Phys Res. A* **544**, 48–54.

Tabak, M., Hammer, J., Glinsky, M.E., Kruer, W.L., Wilks, S.C., Woodworth, J., Campbell, E.M. & Perry, M.D. (1994). Ignition and high gain with ultrapowerful lasers. *Phys. Plasmas* **1**, 1626–1634.

Temporal, M. & Canaud, B. (2009). Numerical analysis of the irradiation uniformity of a directly driven inertial confinement fusion capsule. *Euro. Phys. J. D* **55**, 139–145.

Temporal, M., Canaud, B. & Le Garrec, B.J. (2010*a*). Irradiation uniformity and zooming performances for a capsule directly driven by a 32×9 laser beams configuration. *Phys. Plasmas* **17**, 022701.

Temporal, M., Canaud, B., Laffite, S., Le Garrec, B.J. & Murakami, M. (2010*b*). Illumination uniformity of a capsule directly driven by a laser facility with 32 or 48 directions of irradiation. *Phys. Plasmas* **17**, 064504.

Willi, O., Barringer, L., Bell, A., Borghesi, M., Davies, J., G.lard, R., Iwase, A., MacKinnon, A., Malka, G., Meyer, C., Nuruzzaman, S., Taylor, R., Vickers, C., Hoarty, D., Gobby, P., J.son, R., Watt, R.G., Blanchot, N., Canaud, B., Croso, H., Meyer, B., Miquel, J.L., Reverdin, C., Pukhov, A. & Meyer-ter-Vehn, J. (2000). Inertial confinement fusion and fast ignitor studies. *Nucl. Fusion* **40**, 537–545.